Crosslinking of Peri-Prosthetic Fibrous Membrane

An Exploratory Study

By

Dominique Fuchs // 1526227

In partial fulfillment for the degree

Master of Science

In Biomedical Engineering,

Tissue Biomechanics and Implants

At the Delft University of Technology,

Faculty of Mechanical, Maritime and Material Engineering

To be defended publicly on Friday, August 27th, 2018 at 13:45

Supervisors:	Prof. dr. ir. Amir Zadpoor	TU Delft
	Dr. ir. Lidy Fratila-Apachitei	TU Delft

TUDelft

Acknowledgements

This research would not have been possible without the support of my supervisor Professor Amir Zadpoor, as well as his colleague Lidy Fratila-Apachitei. The support from various Ph.D. Students has also been invaluable to my research. For this I would especially like to thank Nazli Sarkalkan, Parisa Rahnamay Moshtagh, Angela Oostlander and Monique Schoeman. Handling of experiments was facilitated by Marc Zuiddam at Kavli Nanolabs and Sander Leeflang at the TU Delft Biomaterials lab. A very special thanks to the originator of the research, Edward Valstar. Sadly, I will not be able to present this research to him.

While this thesis work has taken far longer than I had originally anticipated. I am glad to finally bring it to its rightful conclusion. Continuing the research was also not always easy for me because of varying activities that took place outside of the scope of academia. The people I have to thank for supporting my return to this thesis time and time again are of course also not only those academically related to the work. Therefore, I would like to thank my parents and brother for motivation and proofreading support, as well as Marloes Röling, whom I could always count on to work through the countless hurdles of this work.

As my path has continued outside of academia already, I know that my calling is elsewhere. Leaving behind this work feels bittersweet however, as I know the contributions to humanity done in the research fields of biomechanics and materials will likely be far greater than my own outside of this field. I will continue to hold in high regard those that have the skills and grit to work in this competitive, challenging research environment more successfully than I have done it.

Abstract

Aseptic loosening is a major cause of revision surgery in total hip arthroplasties. To slow down, or reverse loosening, tissue engineering interventions could provide solutions. One possible solution is collagen crosslinking, increasing the stiffness of the tissue. This research is a first investigation into UV-induced crosslinking on tissue harvested during revision surgeries. Nanoscale measurements using Atomic Force Microscopy (AFM) show an effect of UV crosslinking on tissue degeneration in vitro. Results are inconclusive in determining whether UV collagen crosslinking is a viable intervention for tissue stiffness in aseptic loosening. This study shows tissue degeneration between measurements. Limiting tissue degeneration could improve future research. Changing measurement methods, such as adding microscale (nanoindentation) measurements or utilizing different AFM probe sizes, could lead to more insights. Also adjusting UV crosslinking conditions could allow future research to pinpoint which intensity and duration maximizes crosslinking effects.

Table of Contents

1. Introduction

The number of hip replacement surgeries are increasing steadily, with the number of operations doubling over the past 10 years in the USA [1]. The number of surgeries to revise loosened implants increased as a consequence as well. This increase is especially prevalent in the age group of 45-54 years old. The increase in revision surgeries in this age group is thought to be due to degenerative arthritis, caused by wear and tear on joints during exercise or strenuous work. This condition signifies a loss of cartilage in joints due to inflammation, leading to joint pain and difficulty moving. It can be treated with steroids, and in severe cases with joint-replacement surgery. This age group is especially important to consider for new treatment options, because they are more likely to outlive implants than older age groups. Patients can require revision surgery due to aseptic loosening, dislocation, deep infection, bone fracture, technical error, implant fracture, or pain. The most frequently occurring reason for revision surgery is aseptic loosening, accounting for almost two-thirds of revision surgery in hip-replacements [2]. Preventing the need for revision surgery, or postponing it, is especially important considering every revision surgery is a major surgery, which increases the likelihood of complications.

Aseptic loosening can be caused by inadequate initial fixation, mechanical loss of fixation over time, or biological loss of fixation around the implant due to wear particles [3]. In all cases the contact between bone and implant is compromised. The resulting fibrous tissue around the implant is called peri-prosthetic fibrous membrane, or interface tissue. This tissue lacks the stiffness of the bone tissue, allowing the implant to move. This movement worsens the condition to the point of requiring revision surgery. During revision surgery, the implant and interface tissue are removed from the patient, and a new implant is placed.

Several approaches to reduce aseptic loosening have been investigated, such as: Reduction of wear particles; modification of inflammatory response; or the reduction of bone-mass-loss [4-6]. These approaches are targeting the *causes* of aseptic loosening. After an implant is loosened there are currently no clinically available alternatives to revision surgery. Alternative treatment methods that are currently being researched are: Minimal invasive surgery –in which the interface tissue is removed and replaced with bone cement– to re-fixate the implant [7], and re-differentiate the peri-prosthetic fibrous membrane into bone tissue to reverse aseptic loosening [8].

Re-differentiation of peri-prosthetic fibrous membrane into bone tissue theoretically reverts the tissue damage from aseptic loosening. Even a partial increase in stiffness could extend the implant's lifetime significantly. Re-differentiation pathways are very complex, and patients have a high biological variability due to the different causes of aseptic loosening. Both of these make the method difficult to develop clinically [8]. A simpler method of restoring tissue stiffness is proposed in this research. If the stiffness of the interface tissue could be increased, similar effects to re-differentiation might be possible. Reverting aseptic loosening is not a likely outcome of this kind of treatment but delaying the onset of its symptoms could delay revision surgery, thereby prolonging the lifetime of the implant and improving the patient's quality of life.

Tissue stiffness is directly related to the biological composition of the tissue. The type and orientation of collagen fibers is the main source of stiffness in fibrous membrane tissues, such as interface tissue [9]. The disorganized, heterogeneous nature of the interface tissue indicates a lack of cohesive collagen structures [10]. One way to influence the type and orientation of the collagen structures is collagen crosslinking. Collagen crosslinking occurs naturally to create interconnected, functionally oriented collagen structures, which increase the stiffness of tissue

significantly. It can also cause collagen structures to become less flexible, in aging of tissue or tissue degeneration due to oxidative stress [11]. Artificial crosslinking of the collagen in the interface tissue has very similar results, leading to stiffer tissue. It does however lack the ability to orient fibers in the way the initial biological process of collagen maturation does.

There are numerous methods of collagen crosslinking [12]. However, because a lot of non-natural crosslinking methods are cytotoxic, they are not useful to investigate for future clinical purposes. Also, a high degree of control over the crosslinking is important because of the variances in the tissue. One method of crosslinking, using UV radiation, is already being used in clinical treatments for pathologies – such as keratoconus [13] – as well as other clinical minimal invasive surgery applications [14, 15]. Because of the availability of information regarding treatments, as well as the control offered by UV crosslinking, it was chosen for this research. Accurate pre-determination of rates of crosslinking in peri-prosthetic fibrous membrane is difficult because of the disorganized and heterogeneous nature of the interface tissue [10]. Therefore, the initial goal of this research is to determine whether UV crosslinking can increase the stiffness of peri-prosthetic fibrous membrane.

2. Materials and Methods

In order to measure improvements in the mechanical properties of peri-prosthetic fibrous membrane due to crosslinking, measurements before and after crosslinking were taken, and compared with measurements of samples that were not crosslinked. This comparison was done to eliminate the effect of tissue degeneration between measurements, as sample degeneration influences stiffness measurements on this type of tissue [10]. Therefore, each experiment was done using two samples in parallel. The first sample was crosslinked, and the second sample was left unaffected as a control, see Figure 1.

The time from defrosting until the end of the second measurement was approximately 2 hours for each sample. The experiment was repeated three times, using a total of six samples. Thus, three crosslinked samples (denoted by X_i for $i = 1,2,3$) and three control samples (denoted by C_i) were measured during the experiment. For all samples two measurements took place, the initial stiffness measurement before crosslinking (t_1), and another measurement after crosslinking (t_2). By comparing the stiffness differences between samples before and after crosslinking, relative stiffness developments could be measured. The full experimental protocol can be found in Appendix A - Experimental Protocol.

Experimental Scheme
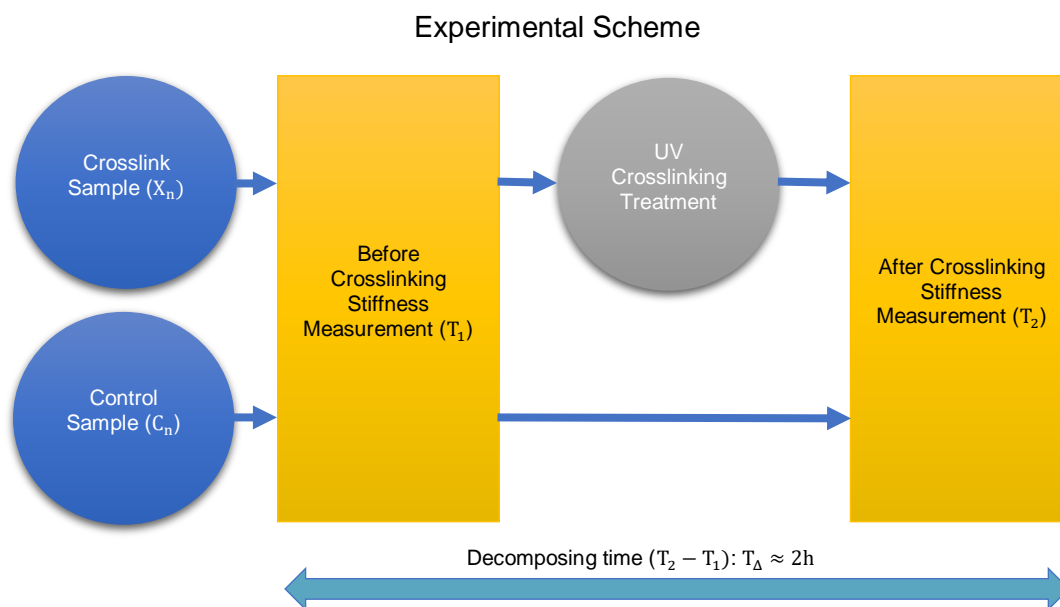
Figure 1: Schematic of experimental proceeding (shown for samples 1 and 2). This process was repeated 3 times for a total of 6 samples.

2.1. Sample Preparation

Tissue samples were harvested during hip implant revision surgery of a 74-year old male patient. The reason for the revision surgery was aseptic loosening of his uncemented hip implant. The implant had ceramic-ceramic contact surfaces and was implanted more than 5 years prior to revision surgery. After surgery, the samples were snap-frozen and stored at $-80°C$ within 24 hours.

In order to prepare samples for Atomic Force Microscopy, flat slices of tissue were needed. This preparation took place at Leiden University Medical Center (LUMC). The tissue was cut into $60\mu m$ slices using a cryo-slicer. Samples were transported by train to the Delft University of Technology (TU Delft). They were kept frozen during transport using dry ice. At the TU Delft Biomaterials Laboratory, the samples were stored at $-28°C$ prior to the experiments.

Image 1 - Leica Cryo-slicer at Leiden University Medical Center. This machine was used to slice $60\mu m$ slices for the Atomic Force Microscopy.

Image 2 - 6-Well plate containing sample cuts and source samples on dry ice, inside transportation box.

Before measurements, samples were taken out of the cold storage and attached to a cell culture dish. They were then rehydrated using a phosphate-buffered saline solution supplemented with a protease inhibitor cocktail, to reduce tissue degeneration during the measurements. Afterwards they were transported to the atomic force microscope in a cooler box at approximately $-4°C$.

Image 3 – Styrofoam box used to transport sample slices on dry ice to TU Delft from Leiden University Medical Center.

2.2.   Measurements

There are several methods to measure mechanical properties of tissue. The main choice of measurement method is based on the scale of measurement. For macro-scale measurements, hardness can be measured by indentation, and stiffness by tensile test. On micro-scale tissue measurements, nanoindentation is commonly used. On a nanoscale, atomic force microscopy can be used. Previous research into peri-prosthetic tissue offers comparison data for nanoindentation and atomic force microscopy. Because the crosslinking of collagen occurs on a nanoscale, and collagen fibrils have been tested on this scale before [16], atomic force microscopy was used for the stiffness measurements in this experiment.

Schematic view of Atomic Force Tapping Mode
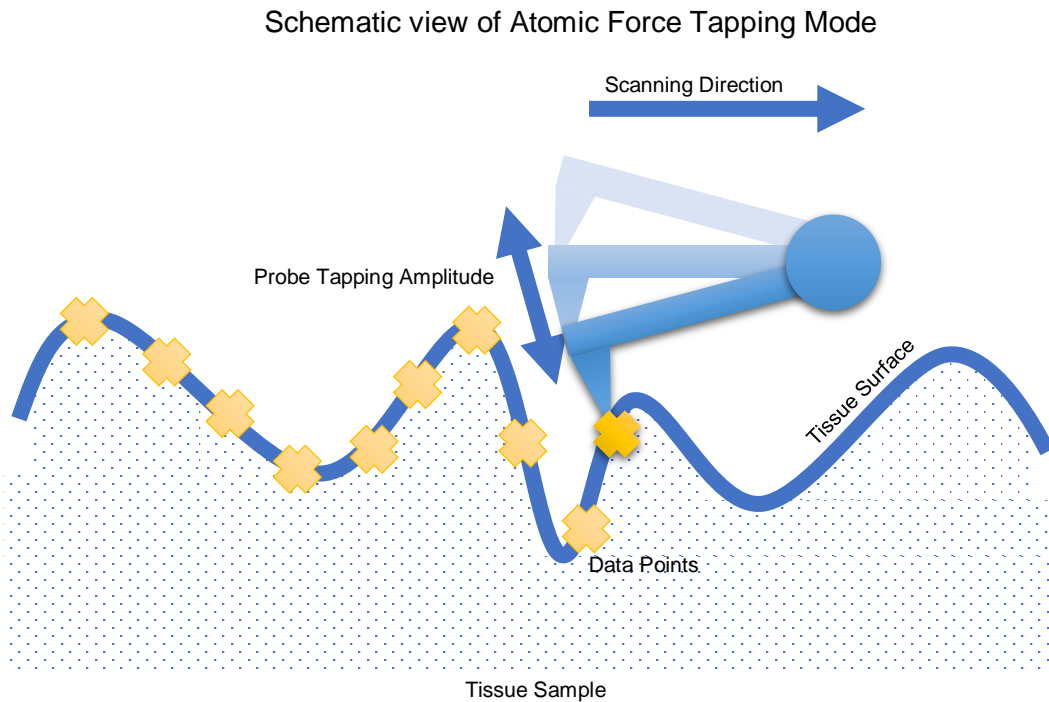
Figure 2: Schematic representation of Atomic Force Microscopy tapping mode. As the probe head indents the surface it moves across the scan direction, measuring indentation curves during each tap.

Atomic force microscopy is a measurement method that uses piezo-electric actuation combined with cantilevers to measure mechanical, topological, or electrical properties of material on a nanoscale. It is a specific form of scanning tunneling microscopy. Because of the scale of measurements and the ability to measure in fluids this is a highly useful measurement method to determine mechanical properties on nanoscale surfaces.

The so-called tapping mode atomic force microscopy method was used in this experiment. In this mode the tip of the probe repeatedly taps the surface of the sample, registering force-displacement curves for each indentation, see Figure 2.

AFM (Bruker Dimension FastScan™, USA [17]) force volume measurements were done at the Kavli Nanolabs at the TU Delft (see Image 3 for the measurement setup). A proprietary tapping mode protocol (Peakforce QNM™, Bruker, USA [18]) was setup using the provided software suite (Nanoscope, Bruker, USA [19]), in conjunction with Silicon Nitride cantilevers (Budgetsensors, USA [20]). This protocol was chosen after initial testing for within-liquid atomic force microscopy. It allows reliable calibration within fluid and offers high measurement speed. This reduces the time between the two measurements, reducing the effect of tissue degradation on the results.

The pyramid-shaped cantilevers had a force-constant of 0.06N/m, and a tip-radius of <15nm. Scans were done on 1μm x 1μm areas of the samples, in a room temperature environment. The measurement area was subdivided into 64 measurement lines of 64 indentations. Input gain and z-limit (movement limit) of the probe were optimized automatically during scans (using ScanAsyst©, Bruker, USA [21]). The scan speed was 1 Hz (1 line per second). At least two locations were measured on each sample, to ensure enough variation in the results due to the heterogeneity of the sample surface.
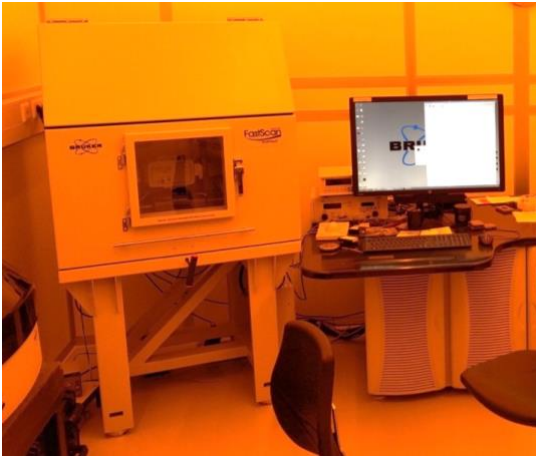
Image 3: The Atomic Force Microscopy setup at the Kavli Nanolabs. The scanner is contained in the chamber on the left, to protect it from external noise/vibration. The computer on the right contains the measuring software and is used to conduct the experiments.
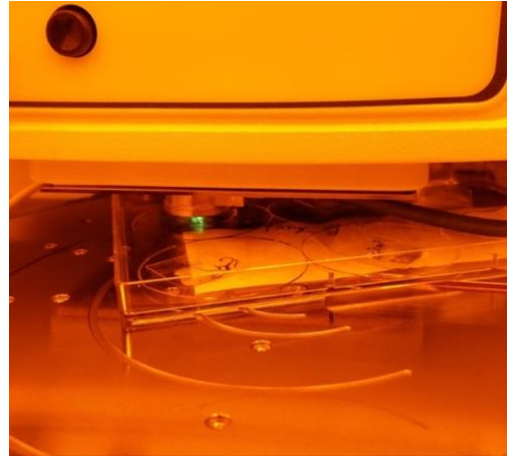
Image 4 – Close-up of scanner head during preliminary experiments. More images of the test-setup & laboratory can be found in Appendix B - Photos of test-setup & Laboratory.

UV crosslinking provides an accurate way to control crosslinking rates compared to chemical crosslinking methods, because UV exposure time and intensity can be controlled accurately. Also, cytotoxicity is reduced because no cytotoxic chemical is left in the tissue. On the other hand, a chemical crosslinker that is gaining popularity due to its biocompatibility and stability is proanthocyanidins [22, 23]. The use of proanthocyanidins was considered, but due to the possibility of unintended side effects on living tissue such as the increase in fibroblast activity [24], which could lead to faster osteolysis, ruled out this method for the current research. Strong UV radiation can also damage tissue, or crosslink other components than collagen [25]. Because of the limited exposure time, however this was considered acceptable. Samples were prepared for crosslinking by flushing the sample container with a stock solution containing 0.05% riboflavin, replacing the original stock solution with the photo-activator solution. Then, to crosslink the samples, they were exposed to 60 seconds of UV light under a 150 mW/cm^2 light source, for a total energy transfer into the tissue of 4.5 J/cm^2.

Image 5 – UV Floodlight used for crosslinking in the Biomaterials laboratory at TU Delft

Image 6 – Close-up of UV Floodlight used for crosslinking in the Biomaterial laboratory at TU Delft.

2.3.   Analysis

Force displacement curves were converted into stiffness values using Nanoscope Analysis (v. 1.40) software. The Young's Modulus (E) was extracted from the force-displacement curves using Sneddon's Modulus Formula:

$$E = -\pi F \frac{v^2 - 1}{2\delta^2 tan(\alpha)}$$

[1]

Where E is the Young's Modulus, F is the tapping force, v is the Poisson's ratio, which is set to 0.5, since the tissue is assumed to be incompressible as in previous research [10], δ is the displacement and α is the half-angle of the conical tip of the probe.

Stiffness values for each AFM measurement were visualized as probability distributions, using normalized histograms. The histograms were normalized by dividing the occurrences by the total number of values measured, to show the probability of the stiffness values.
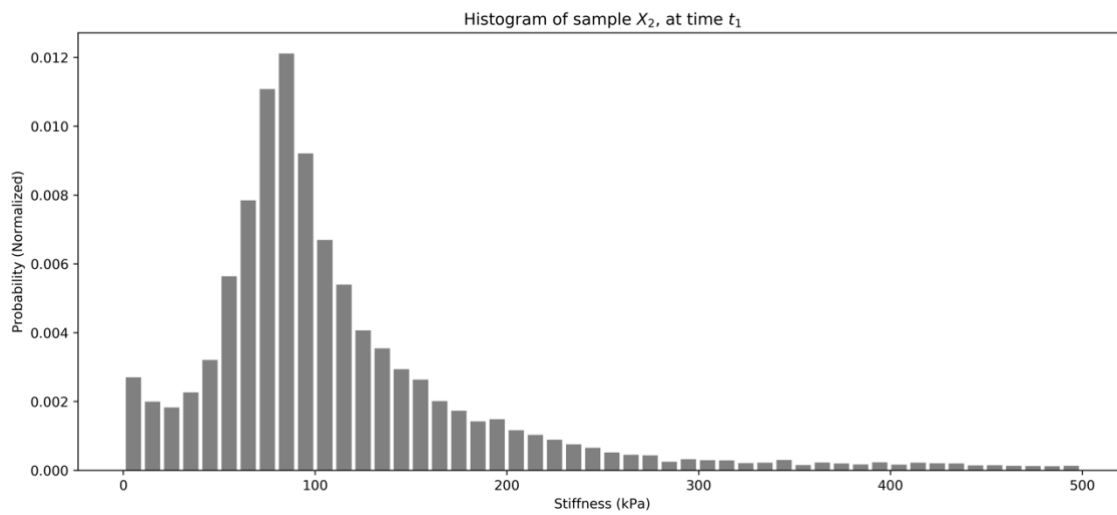
Figure 7: Example of measurement probability distribution, for the first measurement of crosslinked sample 3.

In order to determine the efficacy of the collagen crosslinking, the data-points need to be clustered into their biological constituents. Before this can be done however, the data was prepared for the analysis.

Noise was filtered out to focus on the main tissue components. Signal noise was calculated based on the distribution of the data [26]. This value was then used as a cutoff point, to filter off noise. An example of this is shown in Figure 8 for sample X_3 at t_1, before crosslinking, note the logarithmic scale of the probability. This removes the right-tailed-ness of the distribution, which is likely due to signal noise over a much larger stiffness range than the main measurements.
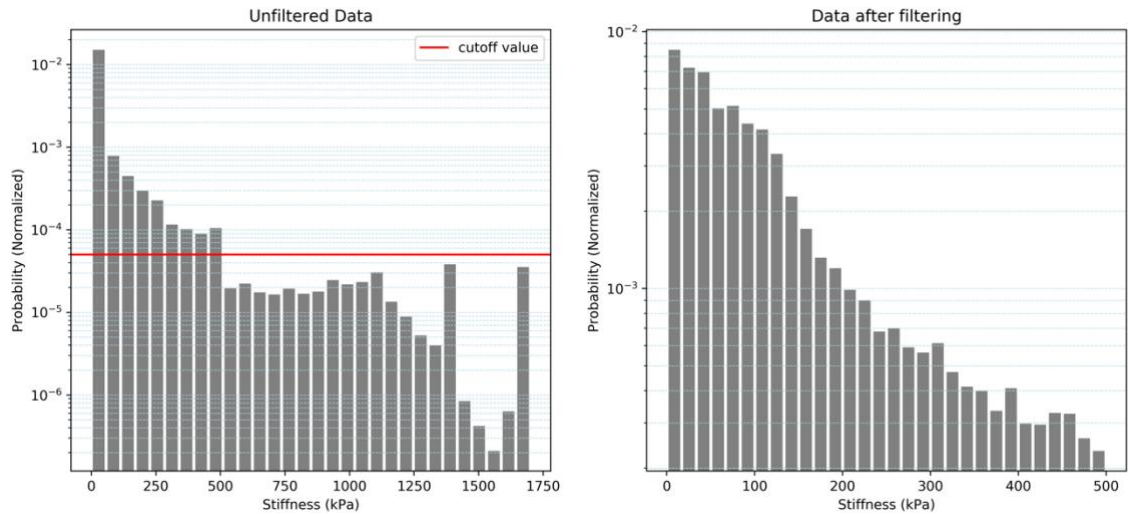
Figure 8: Data filtering example using a cutoff value set by the SNR ratio of the data. The left picture shows the original distribution, as well as the cutoff value. The right figure shows the distribution after filtering. The sample seen here is $X_3 t_1$.

In order to identify the constituents of the tissue, Gaussian Mixture Modeling was applied. The measurements are fitted to several Gaussian components which are expected to relate to the physical components of the tissue [10, 27]. The equation for the components is

$$f(x) = \sum_{i=1}^{m} w_i N(\mu_i, \sigma_i) \qquad [2]$$

where i is the component number, w_i is the i-th component weight, and N denotes the Gaussian (normal) distribution defining the component with a mean of μ and a standard deviation of σ. Figure 9 shows an example of Gaussian mixture modeling on a synthetic example dataset generated with 2 normal distributions. This could of course be done with any number of components. An example fit for 2, 6 and 12 components on real data can be found in the Appendix D - Additional Plots, specifically Figure 16.
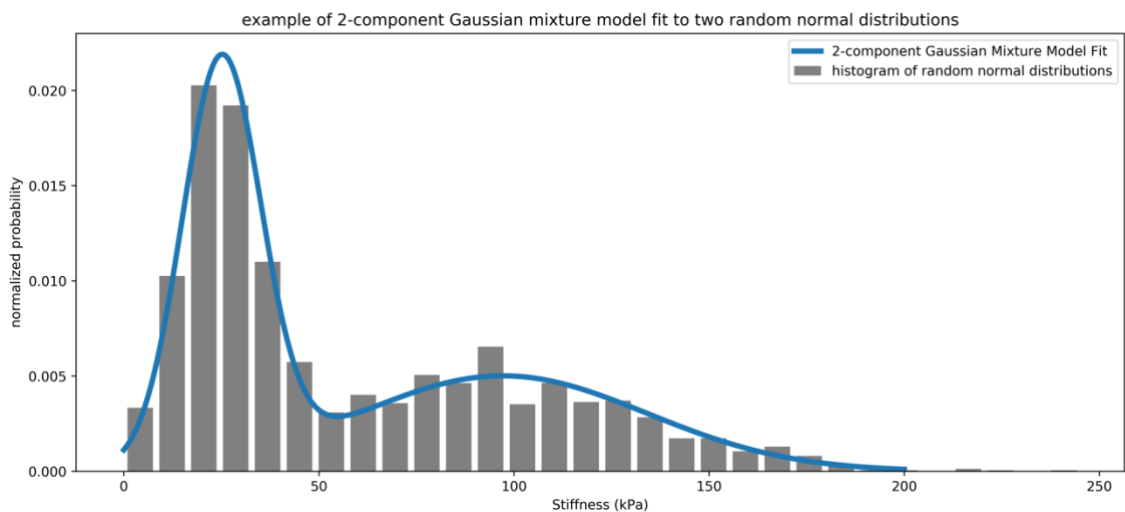
Figure 9: Example of Gaussian mixture modeling on a dataset consisting of 2 pseudorandom normal distributions. The two distributions have mean values of resp. 25 and 90. Because the gaussian mixture model is fit with 2 components it matches the input data well and can be used to determine the means of the original distributions.

The number of components that need to be fit needs to be known before applying gaussian mixture modeling. Based on the biological composition of the tissue, two components are

expected to represent the data [28], which are Collagen and Glycosaminoglycans. On the other hand, instead of relying on a-priori expectations, statistical methods such as the Calinski-Harabasz, Davies-Bouldin, and Silhouette criteria can also be used to identify the optimal number of mixture components. A detailed overview of the clustering indices can be found in Appendix C - Clustering Indexes.
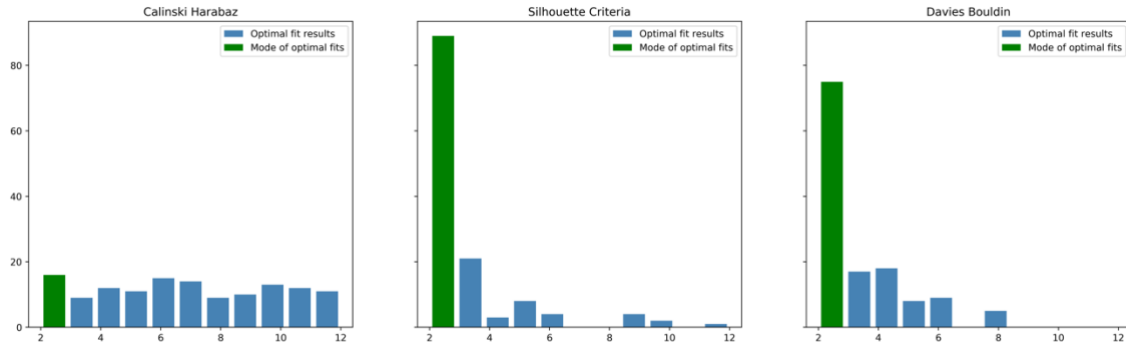
Figure 10:Results of the different criteria evaluated for 2-12 components. Mode of all results combined is 2, which means that considering all criteria equally valid the optimal number of components to use for gaussian mixture modeling is 2 components.

In order to compare component peaks across samples it is important to use the same number of components for each sample. Therefore, in this research we choose the most frequently occurring optimal component number (across all three metrics) to calculate resulting component stiffnesses. After analyzing the fit with up to 13 components for each metric, it was found that the optimal number of components is 2. This matches the a-priori estimation based on the biological composition of the tissue. This also allows us to consider one component to be representing the high-stiffness biological components and the other to represent the low-stiffness biological components.

3.   Results

The experiments were carried out during the summer of 2016. Due to availability of the measurement equipment and opening hours of the faculty the measurements did not always take place at the same time of day. Probe changes were necessary between several measurements due to contamination of the probe (tissue getting stuck to the probe during measurements), probes breaking during probe change, and probes breaking during calibration due to operator error or calibration errors. No clear difference between measurements with 'fresh' probes and used probes could be discovered. Calibration times varied between 1 and 15 minutes. Measurements took place during approximately 25-30 minutes after calibration, while setup/changes between samples took about 5 minutes.

3.1.   Sample size

To guarantee statistical significance of the analyzed datasets they must contain enough samples after denoising. To this extent the percentage of removed samples was considered. These percentages can be found in Figure 11. Sample $C_1 t_1$ has received additional filtering due to an unexpectedly high stiffness spike that can be observed in this dataset (See Figure 12 for the dataset including spike). The $C_1 t_1$ dataset contained stiffness values ranging up to 2MPa where the other datasets were confined to up to 500KPa ranges. It is believed this spike is due to sample contamination.
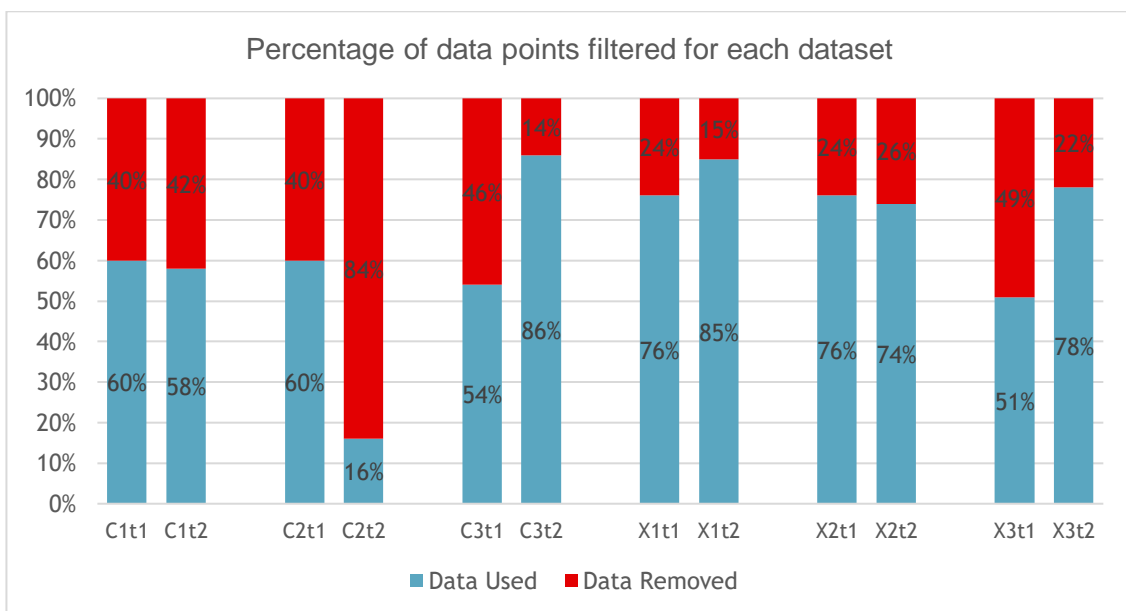
Figure 11: Percentage of data-points removed during filtering, by sample and time. The minimum amount of data truncated from a measurement is 14% from sample $C_3 t_2$. The maximum amount of data truncated is 84% from sample $C_2 t_2$.
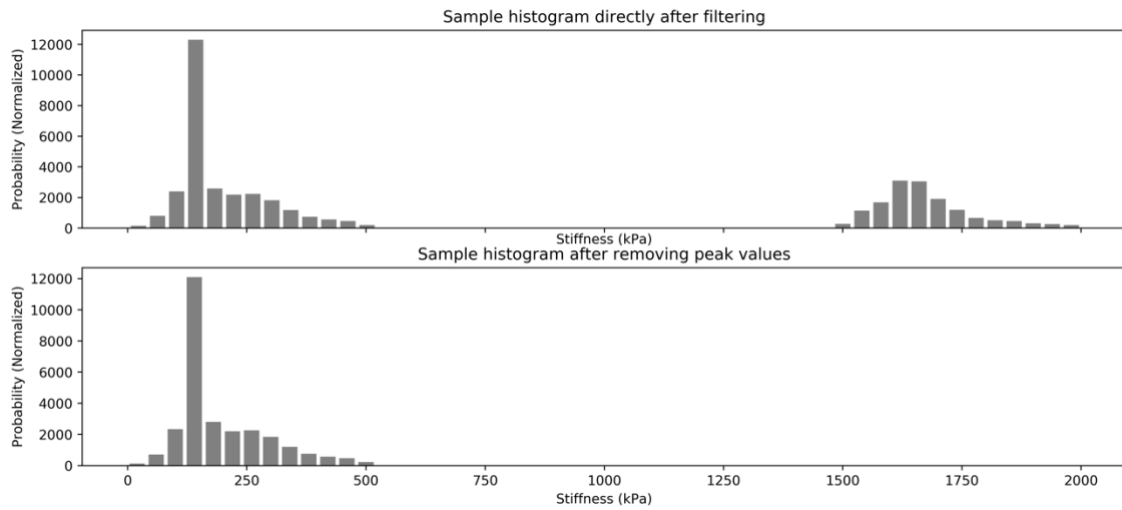
Figure 12 - histogram of sample $C_1 t_1$ showing the before and after view of the contamination filtering

3.2.   Gaussian Mixture Modeling Results

After fitting the two-component Gaussian mixture model to the probability density distribution of the data, the results were plot for each sample and measurement time. Component 1 is the component with lowest mean stiffness, while component 2 is the higher-stiffness component. The Gaussian mixture models are shown superimposed over the data on which they are based in Figure 13. The most important indication of degeneration of the biological tissue is a shift in peaks to the left (lower stiffness) between t_1 and t_2. Conversely, if the peak at t_2 is to the right of the peak at t_1 then that means that the tissue became stiffer between measurements. Because the lines representing the gaussian components are superimposed on top of the data (shown as histograms), it can also be evaluated how well the model matches the data.

Mean values (peaks) of each component at time 1 and time 2 are shown in Table 1. The difference between both values, which shows the stiffness degradation between time 1 and time 2, is also shown in that table.

Table 1: Overview of the mean stiffness values of the Gaussian mixture components, as well as the difference between component mean values on t_1 and t_2. All values are in kPa.

	Component 1 (kPa)			Component 2 (kPa)		
	t_1	t_2	*Difference*	t_1	t_2	*Difference*
X_1	42.00	38.41	*-3.59*	192.44	131.95	*-60.49*
X_2	87.85	75.26	*-12.59*	238.89	287.13	*48.24*
X_3	62.03	65.43	*3.40*	256.08	272.86	*16.78*
average	63.96	59.70	*-4.26*	*229.14*	230.65	1.51
C_1	145.29	101.96	*-43.33*	230.75	230.20	*-0.55*
C_2	105.63	64.54	*-41.09*	818.24	310.07	*-508.17*
C_3	72.34	36.46	*-35.88*	252.33	212.12	*-40.21*
average	107.75	67.65	*-40.10*	433.77	250.80	*-182.98*
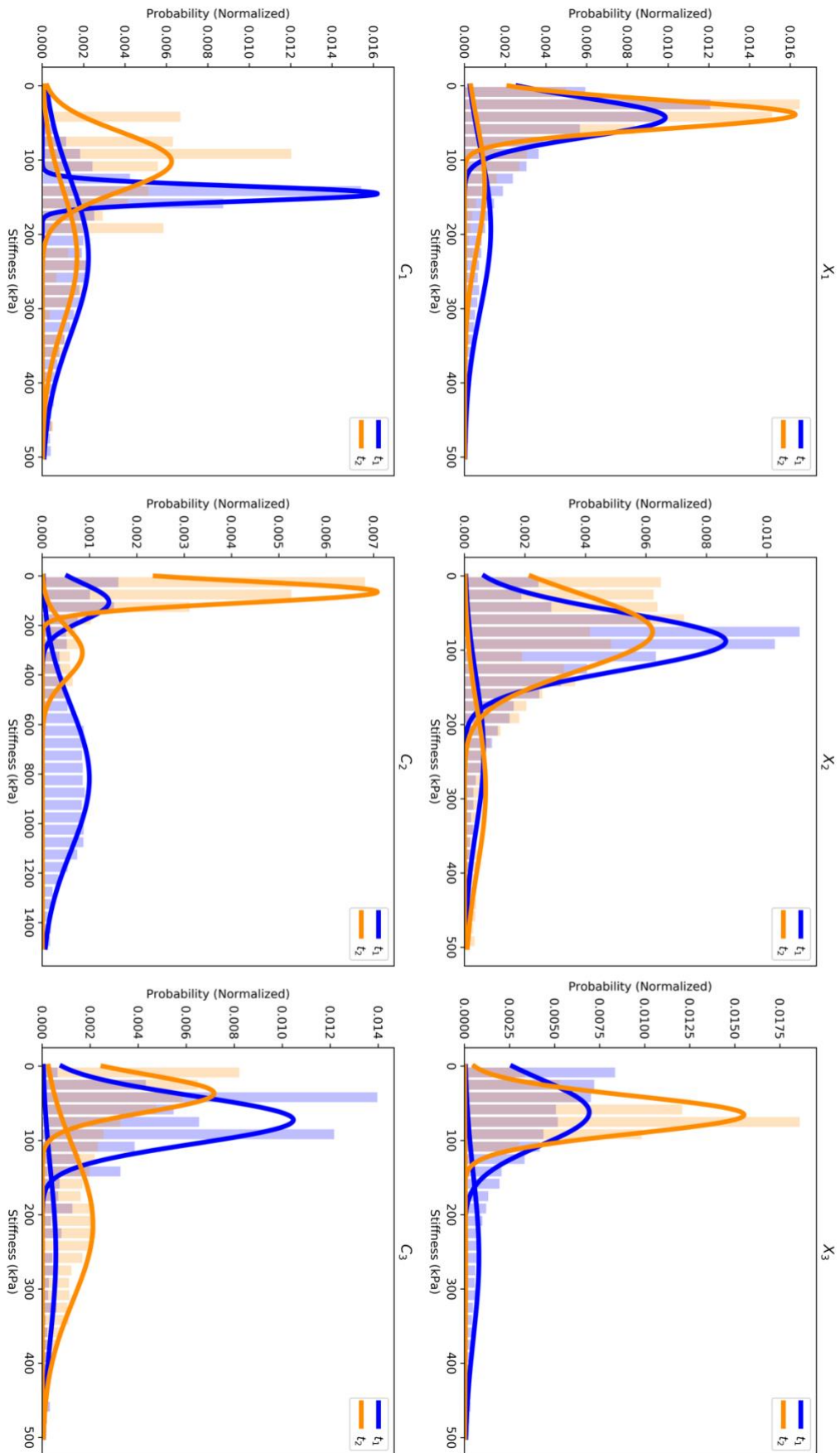
Figure 13: Results showing probability density plots for all the samples, as well as the Gaussian Mixture Models superimposed on top. The top row shows the crosslinked samples, and the bottom row shows the control samples.

Thanks to the gaussian mixture model, it is possible to assign the data-points of each sample to a component. By plotting the data-points by component instead of by sample, an overall trend can be visualized more clearly. This can be seen in Figure 14. A lowering of average stiffness for both components at t_2 compared to t_1 can clearly be seen in the control samples.
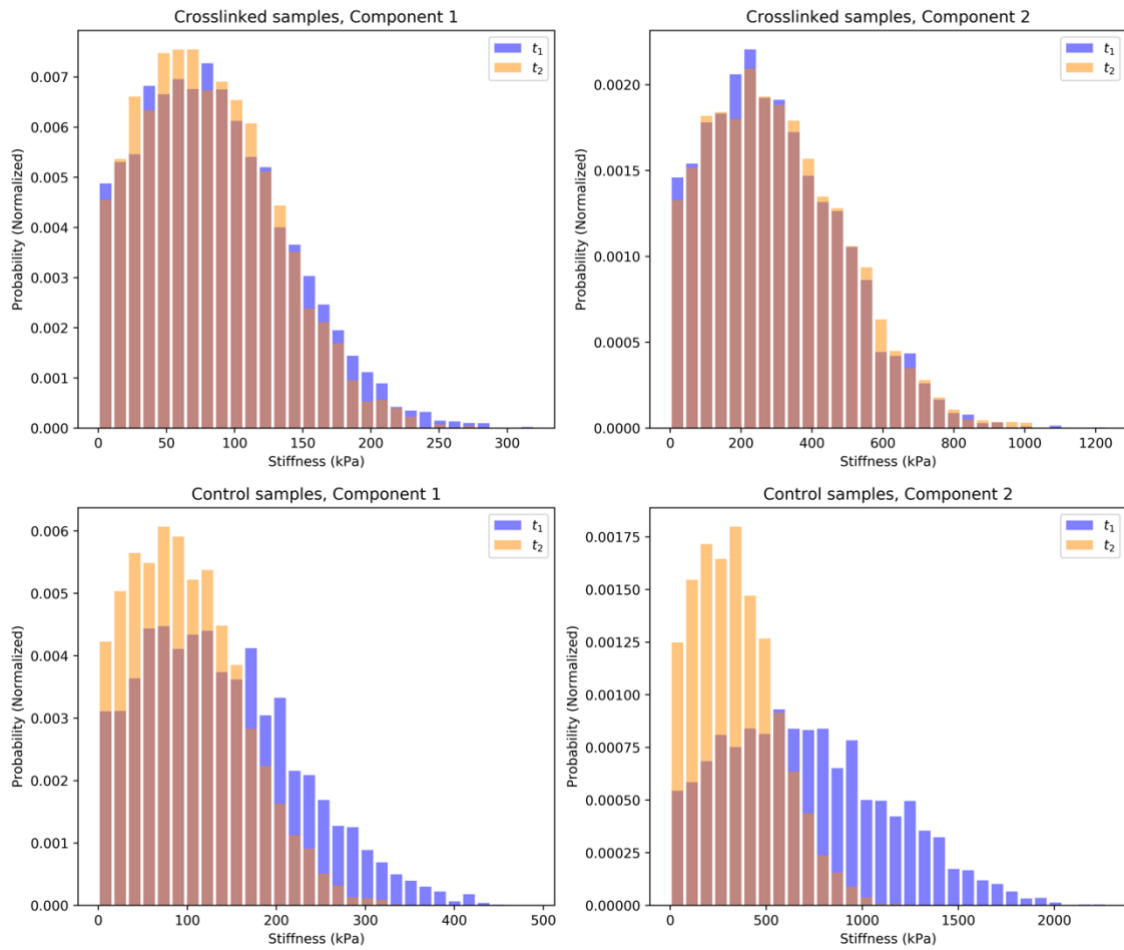
Figure 14 -Combined data points for all crosslinked (X_1, X_2, X_3) and control (C_1, C_3) samples separated by components based on the gaussian mixture modeling. This can be used to evaluate trends between t_1 and t_2 on a more general level.

4.   Discussion

One of the challenges of this research was not technical in nature. The coordination of samples, measurement devices and laboratory space were initially unforeseen. This occurred mainly due to working with 4 different organizations (LUMC Leiden, UMC Utrecht, TU Delft, Kavli Nanolabs) and their respective research groups. The interdisciplinary nature of this research, concerning biological, clinical, physical and chemical themes, also meant that a lot of information and procedures needed to be retrieved from relevant experts in their respective fields. Communication between these different stakeholders was hampered by the various technical terms used that are specific to each field. A lot of the information needed is specific to laboratories, as often equipment and established procedures are specific to departments, and not always equal to the information available in literature. Lacking clinical experience, the sample processing and measurement were far more difficult tasks than anticipated. Therefore, a lot of time was used in setting up a stable process in calibration and measurements. This time could have more fruitfully been spent on additional measurement (from different patients) or doing additional experiment in different scales, such as nanoindentation measurements. The turnover of information and access to materials/laboratories due to Ph.D. and Master Students finishing their theses and leaving the departments also added some difficulty to finishing the experiments and added a limit on the amount of measurements preformed. These challenges have no scientific or technical basis but are surely not unique to the specifics of this research, and therefore worth mentioning. Interdisciplinary research offers the possibility to further disciplines in ways that cannot be done from within a discipline. They therefore strongly benefit from logistical and organizational support and can be promoted by simplifying the coordination and knowledge exchange.

4.1.   Data Quality

Noise filtering shows a relative high degree of noise in all samples, although more than half of the data-points were valid for all samples except C_2 at t_2. Sample C_2 was the noisiest sample of all samples. Results stemming from this sample should therefore be evaluated critically. No problems were observed during the tests that could impact the validity of this measurement. Also, visual inspection of the probability density distribution does not indicate invalid data, although component 2 stiffness values are noticeably higher than in other control samples.

Large variations between samples at t_1, before any changes that relate to degradation or crosslinking could explain differences, make precise comparisons difficult. This, combined with the large amount of filtered out data points shows that the measurement method might not be optimal. More experimentation into different atomic force microscopy modes, or even development of a custom protocol was however not possible within the time available for this research. This is also the reason why effects are evaluated qualitatively instead of quantitatively, since the data does not offer enough foundation for quantitative claims.

Stiffness values are similar to previous results from AFM measurements on this type of tissue. They are generally low when compared to results from other tissue that has a high collagen content. This has previously been associated with the lack of organization in the collagen, and the ultimate failure of the tissue resulting in revision surgery [10].

4.2.   Experimental Results

The observed Young's Modulus values in general match previous studies on this tissue, which show a range of $0 - 250\ kPa$. This stiffness can be considered relatively low compared to

other measurements of soft connective tissue using AFM, such as aortic wall tissue ($0.025\ MPa$), scar tissue ($1.5\ MPa$), normal skin tissue ($0.5\ MPa$), and pericardium ($25\ MPa$) [29-32].

In previous research with cartilage glycation, crosslinking did not lead to a significantly higher collagen stiffness, but rather a reduced degeneration of collagen [33]. The lack of clear degeneration in combined values from crosslinked samples is in line with these results. The control samples show a clear degeneration between t_1 and t_2, which is not present in the combined crosslinked samples. Separately, not all samples match this pattern completely or in the same degree. This possibly indicates that the crosslinking process has a high variance. Longer crosslinking times could help reduce this variance. This will also increase the degeneration of control samples, making a clearer case for these results possible. Difference in stiffness changes between samples can also be explained by the organization of the collagen fibers. This has shown to result in a high variance of stiffness, but also reduces the effect of crosslinking when collagen fibers are not close enough to each other to chemically bond during the UV light exposure. Both of these effects can lead to very non-uniform results and crosslinking effects.

The absolute stiffness values show a high variance in measured stiffness for both the control and crosslinked values. Component 1 stiffness values are in the range of $40 - 145\ kPa$, while component 2 stiffness values (leaving out extreme values) range from $130 - 310\ kPa$. This shows some overlap, although the range of component means is small enough to clearly discern the components for each sample. Comparing average component 1 and 2 peak values ($\mu_{1,average} = 74.77\ kPa$, $\mu_{2,average} = 286.09\ kPa$) to previous results on osteoarthritic cartilage, where a proteoglycan peak of $22\ kPa$, and a collagen peak of $384\ kPa$ was identified, as well as previous research on peri-prosthetic fibrous membrane, with a ground substance peak of $19\ kPa$ and a collagen peak of $203\ kPa$, the two components identified could match these biological components as well. Differences in ground substance makeup as well as collagen orientation can have a large effect on these results as well [10].

4.3.   Limitations of experiments and Recommendations for future research

Limiting the experiments to atomic force microscopy measurements both removes context that could serve the analysis, as well as limit the comparison to other studies done on the tissue. Peri-prosthetic fibrous membrane has been well researched on macro-scale [34]. Viscoelastic models have been established based on the data, and this could have been a valuable avenue to extend crosslinking results to. Microscale measurements from nanoindentation tests also exist for this type of tissue [10]. Again, a comparison between crosslinking results and previous results would have been valuable. Proving the effect of crosslinking on the tissue stiffness might have been possible more conclusively on different topological scales. Limiting the study on measurements at a single scale simplified the analysis but might have left out important effects, such as the effect of hierarchical tissue organization on crosslinking, which could have been measured by varying the geometry of the probe or using nanoindentation measurement [35-38].

Biochemical changes due to degeneration and crosslinking can also lead to stiffness changes in different parts of the nonlinear stress strain curve of collagens fibrils, as observed in computational studies [39]. It is however unlikely that this has affected the research strongly, since similar tests have been done with this tissue before. The effect of increased breakage in collagen fibers after crosslinking could also lead to a misrepresentation of results. This effect has not been studied however, and tapping forces are significantly lower than breaking stresses observed in other articles [40]. UV Light can also have a degenerative effect on

certain tissue components [25, 41]. This could explain increased general variance of results after crosslinking.

Another limitation of the research is the use of samples from a single patient. Though an effect was observed, it is not certain that this effect will be qualitatively the same for other patients. Further research into this is thus required. The time between tissue harvest and storage at the LUMC is not recorded, and this could vary between patients based on surgeon and surgery duration. If this experiment is repeated with samples from other patients this could lead to different results as well.

The methods used were chosen in accordance with literature in tissue biomechanics and clinical fields that deal with collagen-rich connective tissue (such as orthopedic, dental and vision surgery). The many different ways of using atomic force microscopy for biological tissue warrant a deeper look at the methods, and how they relate to other measurement methods, which might not have the drawbacks discussed in the previous section.

Atomic force microscopy allows the measurement of fully submerged tissue samples. This simulates an in-vivo situation, but the adhesion of the tissue on the substrate can affect tissue mechanics to some extent. Also, some calibration issues caused the measurements to take longer than dry measurements would have taken. Some research uses dry and/or semi-wet measurements for connective tissue [42], this could save time in calibration, likely resulting in 'fresher' tissue measurements. The effect of a dry environment lacking enzymatic inhibitors on degeneration has not yet been investigated. If it would be shown to promote less degeneration this could increase the difference even more.

There are a large number of different tissue crosslinking methods that could have been used in this research. In order to promote the clinical use of tissue crosslinking this research focused on a non-cytotoxic method [43, 44]. Using a method proven to strongly crosslink the tissue would have also possibly showed a clearer effect, thus serving as initial prove of tissue alteration, before searching for methods with low cytotoxicity and replicating the (larger) effect. Glycation has been thoroughly investigated in relation to cartilage degeneration and has shown to have no significant effect on bone tissue, whereas the effects on stiffness in soft tissue is pronounced [45, 46]. Non-enzymatic glycation with l-threose has previously been used on cartilage with very high stiffness increases (up to 12x on nanoscale) [33]. Thus, l-threose would seem to be a very promising crosslinker to be used in this tissue and application. Peri-prosthetic fibrous membrane does however not lend itself well to incubation in vitro, because of the extreme degeneration that it will undergo compared to cartilage. Also, cartilage is a more homogenously organized tissue, and therefore will likely show better results for all different crosslinking methods.

Clarifying the effects of the crosslinking methods on separate components, such as collagen and proteoglycans, will help explain the results seen in this tissue. Building up knowledge from a bottom-up approach like this will allow for easier forecasting of crosslinking results based on different tissue types and consistencies. Experimenting on tissues will however consider the complexity of the tissue, and possibly interactions with cells and other minor components into account, that could influence results in a major way. Therefore, it is hard to say whether the approach used here lacked the fundamental knowledge to explain the crosslinking results, and would greatly benefit from such foundational experimentation, or whether the complexities of the tissue make such inference too difficult.

Having access to dedicated process experts to help setup the experimental protocol that might be best to show specific effects could help improve results of future research in this field. Standardized analytical methods could help speed up data analysis from experiments, and comparison between research groups. A lot of theoretical knowledge is exchanged through literature, but practical implementation of standards is lacking. Setting up an

optimized scan protocol could reduce noise and measurement variance, further improving the fidelity of the data. The samples were stored at a location approximately 30km from where the experiments took place. Reducing this distance, or processing the samples locally could reduce degeneration, further improving the quality of data generated.

A final improvement for future research has been mentioned in previous research already. The orientation of the samples with regards to the implant and body of the patients is unknown. This means it is difficult to evaluate the effect of possible fiber orientation on the measurement, and the impact of for example tapping direction of the AFM. If this could be registered for new samples, this could open up new avenues of testing previously impossible to consider. The impact of strain on cell behavior has been researched thoroughly previously and adding to this the mechanical evaluation of peri-prosthetic fibrous membrane could allow for new insights [47, 48].

5. Conclusion

Measurements of tissue stiffness using the AFM method described in this work are inconclusive at quantifying the herein mentioned crosslinking method. However, it can be shown that UV Crosslinking can reduce the degeneration of peri-prosthetic fibrous membrane. Unfortunately, other tissue interactions, such as crosslinking of non-collagen proteins, or degeneration of the tissue as a whole might have affected the results. This indicates that further detailed research might be necessary to determine the usability of UV crosslinking in a clinical setting. Because of the heterogeneous nature of the tissue, a more sample independent crosslinking technique might be more valid.

The limitations of this study mean that the value for further research into treatment options for aseptic loosening is also limited. It might however inspire more research into this complex field, given that most advances are driven from a clinical perspective and not an engineering perspective, while this field also benefits from the chemistry and engineering approaches attempted.

The step from molecular biology to tissue biology is a complex and difficult step, and a lot of simplifications used in this research have led to an unclear picture of what really happens when UV-crosslinking peri-prosthetic fibrous membrane. Smaller, easier to control experiments relating to the different aspects of UV crosslinking could prove more insightful in the future. The effect on (chemical) stability of the tissue, or the effect of UV radiation on separate chemical constituents of the tissue, are next steps that should be considered.

Bibliography

[1] AJRR, "American Joint Replacement Registry Report 2016," in "American Joint Replacement Registry Annual Report," American Joint Replacement Registry, Rosemont, IL2017.

[2] G. Garellick, J. Kärrholm, H. Lindahl, H. Malchau, C. Rogmark, and O. Rolfson, "The Swedish Hip Arthroplasty Register," 2014.

[3] Y. Abu-Amer, I. Darwech, and J. C. Clohisy, "Aseptic loosening of total joint replacements: mechanisms underlying osteolysis and potential therapies," (in eng), *Arthritis Res Ther,* vol. 9, no. Suppl 1, p. S6, 2007.

[4] A. B. Pedersen and A. M. Fenstad, "Nordic Arthroplasty Register Association Report," ed, 2016.

[5] G. Mbalaviele, D. V. Novack, G. Schett, and S. L. Teitelbaum, "Inflammatory osteolysis: a conspiracy against bone," (in eng), *J Clin Invest,* vol. 127, no. 6, pp. 2030-2039, Jun 01 2017.

[6] L. Cavalli and M. L. Brandi, "Periprosthetic bone loss: diagnostic and therapeutic approaches," (in eng), *F1000Res,* vol. 2, p. 266, 2013.

[7] G. Kraaij, G. J. Tuijthof, J. Dankelman, R. G. Nelissen, and E. R. Valstar, "Waterjet cutting of periprosthetic interface tissue in loosened hip prostheses: an in vitro feasibility study," (in eng), *Med Eng Phys,* vol. 37, no. 2, pp. 245-50, Feb 2015.

[8] M. A. E. Schoeman, A. E. Oostlander, K. E. Rooij, E. R. Valstar, and R. Nelissen, "Peri-prosthetic tissue cells show osteogenic capacity to differentiate into the osteoblastic lineage," (in en), *J Orthop Res,* vol. 35, no. 8, pp. 1732-1742, Aug 2017.

[9] R. H. Pritchard, "Investigations into the Mechanics of Connective Tissue," ed, 2015.

[10] A. Moerman, "Structural and Mechanical Characterization of the Peri-Prosthetic Fibrous Membrane," ed, 2015.

[11] M. G. Haugh, M. J. Jaasma, and F. J. O'Brien, "The effect of dehydrothermal treatment on the mechanical and structural properties of collagen-GAG scaffolds," *J Biomed Mater Res A,* vol. 89, no. 2, pp. 363-9, May 2009.

[12] D. Fuchs, "Literature Study: Biochemical Factors that alter the mechanical properties of connective tissue," Literature, Tissue Biomechanics and Implants, TU Delft, 2018.

[13] A. B. Cummings, R. McQuaid, and M. Mrochen, "Newer protocols and future in collagen cross-linking," *Indian J Ophthalmol,* vol. 61, no. 8, pp. 425-7, Aug 2013.

[14] N. Lang *et al.*, "A Blood-Resistant Surgical Glue for Minimally Invasive Repair of Vessels and Heart Defects," (in eng), *Sci Transl Med,* vol. 6, no. 218, p. 218ra6, Jan 8 2014.

[15] J. Ren, J. Venugopalan, J. Xu, B. Kairdolf, R. Durfee, and M. D. Wang, "Multi-Channel LED Light Source for Fluorescent Agent Aided Minimally Invasive Surgery," (in eng), *Conf Proc IEEE Eng Med Biol Soc,* vol. 2014, pp. 6927-30, 2014.

[16] M. P. E. Wenger, L. Bozec, M. A. Horton, and P. Mesquida, "Mechanical Properties of Collagen Fibrils," *Biophysical Journal,* vol. 93, no. 4, pp. 1255-1263, 2007/08/15/ 2007.

[17] Bruker, "Dimension Fastscan / The World's Fastest AFM," ed. Santa Barbara, CA, USA, 2011.

[18] Bruker and Y. Hua, "PeakForce QNM - Advanced Applications Training 2014," ed, 2014.

[19] Bruker, "NanoScope Analysis 1.50," ed: Bruker, 2016.

[20] BudgetSensors, "AFM Probe Model: SiNi," ed, 2016.

[21] Bruker, "ScanAsyst / Exclusive, Self-Optimizing AFM Imaging," ed, 2013.

[22] A. K. Bedran-Russo, P. N. Pereira, W. R. Duarte, J. L. Drummond, and M. Yamauchi, "Application of crosslinkers to dentin collagen enhances the ultimate tensile strength," *J Biomed Mater Res B Appl Biomater,* vol. 80, no. 1, pp. 268-72, Jan 2007.

[23] B. Han, J. Jaurequi, B. W. Tang, and M. E. Nimni, "Proanthocyanidin: a natural crosslinking reagent for stabilizing collagen matrices," *J Biomed Mater Res A,* vol. 65, no. 1, pp. 118-24, Apr 01 2003.

[24] Y. Yang, A. C. Ritchie, and N. M. Everitt, "Comparison of glutaraldehyde and procyanidin cross-link scaffolds for soft tissue engineering," *Materials Science and Engineering,* vol. 80, pp. 263-273, 2017.

[25] C. Edwards, A. Pearse, R. Marks, Y. Nishimori, K. Matsumoto, and M. Kawai, "Degenerative Alterations of Dermal Collagen Fiber Bundles in Photodamaged Human Skin and UV-Irradiated Hairless Mouse Skin: Possible Effect on Decreasing Skin Mechanical Properties and Appearance of Wrinkles," *Journal of Investigative Dermatology,* vol. 117, no. 6, pp. 1458-1463, 2001/12/01/ 2001.

[26] *The Essential Physics of Medical Imaging.* 2018.

[27] M. A. E. Schoeman, A. E. Oostlander, K. E. d. Rooij, C. W. G. M. Löwik, E. R. Valstar, and R. G. H. H. Nelissen, "Refixation of loosened hip prostheses: Osteogenic capacity of periprosthetic tissue cells," (in en), 2017-04-01 2017.

[28] A. A. Zadpoor, "Nanomechanical characterization of heterogeneous and hierarchical biomaterials and tissues using nanoindentation: the role of finite mixture models," *Mater Sci Eng C Mater Biol Appl,* vol. 48, pp. 150-7, Mar 2015.

[29] A. E. Oostlander, A. M. Moerman, A. A. Zadpoor, M. A. E. Schoeman, R. G. H. H. Nelissen, and E. R. Valstar, "Structural and Mechanical Characterization of the Peri-Prosthetic Fibrous Membrane," (in en), 2017-04-01 2017.

[30] Q. Li *et al.*, "Micromechanical anisotropy and heterogeneity of the meniscus extracellular matrix," *Acta Biomater,* vol. 54, pp. 356-366, May 2017.

[31] A. Anura, D. Das, M. Pal, R. R. Paul, S. Das, and J. Chatterjee, "Nanomechanical signatures of oral submucous fibrosis in sub-epithelial connective tissue," *J Mech Behav Biomed Mater,* vol. 65, pp. 705-715, Jan 2017.

[32] A. Gimenez, J. J. Uriarte, J. Vieyra, D. Navajas, and J. Alcaraz, "Elastic properties of hydrogels and decellularized tissue sections used in mechanobiology studies probed by atomic force microscopy," *Microsc Res Tech,* vol. 80, no. 1, pp. 85-96, Jan 2017.

[33]   P. R. Moshtagh, N. M. Korthagen, M. H. P. van Rijen, R. M. Castelein, A. A. Zadpoor, and H. Weinans, "Effects of non-enzymatic glycation on the micro- and nano-mechanics of articular cartilage," *J Mech Behav Biomed Mater,* vol. 77, pp. 551-556, Jan 2018.

[34]   G. Kraaij, A. A. Zadpoor, G. J. Tuijthof, J. Dankelman, R. G. Nelissen, and E. R. Valstar, "Mechanical properties of human bone-implant interface tissue in aseptically loose hip implants," *J Mech Behav Biomed Mater,* vol. 38, pp. 59-68, Oct 2014.

[35]   J. H. Lindeman *et al.*, "Distinct defects in collagen microarchitecture underlie vessel-wall failure in advanced abdominal aneurysms and aneurysms in Marfan syndrome," *Proc Natl Acad Sci U S A,* vol. 107, no. 2, pp. 862-5, Jan 12 2010.

[36]   R. Oftadeh, B. K. Connizzo, H. T. Nia, C. Ortiz, and A. J. Grodzinsky, "Biological connective tissues exhibit viscoelastic and poroelastic behavior at different frequency regimes: Application to tendon and skin biophysics," *Acta Biomater,* vol. 70, pp. 249-259, Apr 1 2018.

[37]   S. L. Kotova *et al.*, "Early Effects of Ionizing Radiation on the Collagen Hierarchical Structure of Bladder and Rectum Visualized by Atomic Force Microscopy," *Microsc Microanal,* vol. 24, no. 1, pp. 38-48, Feb 2018.

[38]   B. Han *et al.*, "AFM-Nanomechanical Test: An Interdisciplinary Tool That Links the Understanding of Cartilage and Meniscus Biomechanics, Osteoarthritis Degeneration, and Tissue Engineering," (in English), *Acs Biomaterials Science & Engineering,* vol. 3, no. 9, pp. 2033-2049, Sep 2017.

[39]   B. Depalle, Z. Qin, S. J. Shefelbine, and M. J. Buehler, "Influence of cross-link structure, density and mechanical properties in the mesoscale deformation mechanisms of collagen fibrils," *J Mech Behav Biomed Mater,* vol. 52, pp. 1-13, Dec 2015.

[40]   V. R. Sherman, W. Yang, and M. A. Meyers, "The materials science of collagen," *J Mech Behav Biomed Mater,* vol. 52, pp. 22-50, Dec 2015.

[41]   K. S. Weadock, E. J. Miller, L. D. Bellincampi, J. P. Zawadsky, and M. G. Dunn, "Physical crosslinking of collagen fibers: comparison of ultraviolet irradiation and dehydrothermal treatment," *J Biomed Mater Res,* vol. 29, no. 11, pp. 1373-9, Nov 1995.

[42]   H. K. Webb, V. K. Truong, J. Hasan, R. J. Crawford, and E. P. Ivanova, "Physico-mechanical characterisation of cells using atomic force microscopy - Current research and methodologies," *J Microbiol Methods,* vol. 86, no. 2, pp. 131-9, Aug 2011.

[43]   G. Galietta, L. Di Gioia, S. Guilbert, and B. Cuq, "Mechanical and thermomechanical properties of films based on whey proteins as affected by plasticizer and crosslinking agents," (in English), *Journal of Dairy Science,* vol. 81, no. 12, pp. 3123-3130, Dec 1998.

[44]   A. Pinheiro, A. Cooley, J. Liao, R. Prabhu, and S. Elder, "Comparison of natural crosslinking agents for the stabilization of xenogenic articular cartilage," *J Orthop Res,* vol. 34, no. 6, pp. 1037-46, Jun 2016.

[45]   A. E. M. Jorgensen, M. Kjaer, and K. M. Heinemeier, "The Effect of Aging and Mechanical Loading on the Metabolism of Articular Cartilage," *J Rheumatol,* vol. 44, no. 4, pp. 410-417, Apr 2017.

[46]   G. K. Reddy, "Glucose-mediated in vitro glycation modulates biomechanical integrity of the soft tissues but not hard tissues," *J Orthop Res,* vol. 21, no. 4, pp. 738-43, Jul 2003.

[47]   C. Florea *et al.*, "A combined experimental atomic force microscopy-based nanoindentation and computational modeling approach to unravel the key contributors to the time-dependent mechanical behavior of single cells," *Biomech Model Mechanobiol,* vol. 16, no. 1, pp. 297-311, Feb 2017.

[48]   F. Boccafoschi, C. Mosca, M. Ramella, G. Valente, and M. Cannas, "The effect of mechanical strain on soft (cardiovascular) and hard (bone) tissues: common pathways for different biological outcomes," *Cell Adh Migr,* vol. 7, no. 2, pp. 165-73, Mar-Apr 2013.

Appendix A - Experimental Protocol

Requirements

Equipment

- UV Chamber
- UV protection glasses
- Bruker AFM Dimension FastScan
- FastScan Scanner
- AFM Cantilevers
- Mini cooler box (4°C)
- Ice packs
- Epoxy glue
- Tweezers
- Cell culture dish
- Parafilm
- Autoclavable bags

Reagents

General reagents:

- Human interface tissue samples
- PBS
- Complete protease inhibitor cocktail
- NaN_3

Crosslinking reagents:

- Riboflavin solution
-

Reagent preparation

PBS supplemented with protease inhibitor cocktail (=Stock Solution)

1. Prepare 100mM PBS (pH = 7.0)
2. Add 1 tablet of complete protease inhibitor cocktail into the PBS
3. Stock Solution stable at $2 - 8°C$ for one to two weeks and at $-25°C$ for 12 weeks

Photoactivator Solution

1. Add 0.05% w/v Riboflavin to Stock Solution
2. Prepare as needed, do not store

Transport

For transportation of the specimens from the *Biomaterials Lab* (34-J-0-460) to *Kavli Nanolabs*, and vice versa, steps as detailed in the procedure will be used, aligned with standard procedures detailed in the Biomaterials lab manual.

Procedure

Specimen preparation

1. Unpack the specimens from the 6-well plates which are stored in portable freezer
2. Pick the samples by tweezer
3. Glue the samples with epoxy glue on the substrate
4. Put the mounted specimens into the cell culture dish
5. Add PBS supplemented with a protease inhibitor cocktail and $0.01\% NaN_3$ (Afterwards referred to as 'Stock solution')
6. Seal the dishes with the parafilm
7. Keep the samples at $4°C$ in mini cooler box when they are not being experimented upon
8. Transport the samples to the *Kavli Nanolabs* for Atomic Force Microscopy (AFM) measurements

Trials

1. Transport samples to *Kavli Nanolabs* for AFM
2. Perform AFM Testing (See: AFM Testing)
3. Transport samples to the *Biomaterials Lab* for crosslinking.
4. Perform Tissue crosslinking (See: Crosslinking Protocol).
5. Transport to the *Kavli Nanolabs* is neccesary after crosslinking to proceed with trials.
6. Perform AFM Testing (See: AFM Testing)
7. Transport samples back to *Biomaterials Lab* for disinfection and disposal

AFM Testing

1. Put the sample with tweezers into the AFM fluid cell which prevents the sample from being in contact with the machine
2. Perform indentation tests according to machine specifics using own tip (which is being used exclusively on this tissue)
3. Remove sample with tweezers from the AFM fluid cell into the cell culture dish
   - Repeat step 1-3 for control sample

1. Add photoactivator to sample dish
2. Place sample in UV chamber
3. Activate UV lamp for crosslinking duration: 60 seconds
4. Remove sample from UV chamber
5. Flush sample dish with stock solution to get rid of photoactivator (Riboflavin)
6. Add fresh stock solution to sample dish

Crosslinking Protocol

Disinfecting

Disinfecting at *Kavli Nanolabs*

1. Wipe the working surfaces and tweezers with 70% ethanol before and after working to avoid contamination from any spill of material and following the rules of the Biomaterials Lab/Kavli Nanolabs.
2. Wash the fluid cell with distilled water and then 70% ethanol
3. Collect the tools in autoclave-able bags for further disinfecting at the *Biomaterials Lab*
4. Place the 6-well plates and cell culture dishes in the clean and separated bags to avoid contamination and properly seal them
5. place the samples after tests in autoclave-able bags and properly seal them
6. put the gloves in the autoclavable bags and properly seal them
7. Related to lab suit, use your own specific lab suit. Lab suits will be cleaned and desinfected according to *Kavli Nanolabs* specification

Disinfecting at *Biomaterials Lab*

1. Wipe the working surfaces and tweezer with 70% ethanol
2. Cleaning protocol UV Chamber:
3. Remove sample from UV chamber
4. Turn on UV chamber to disinfect interior
5. Wipe external surfaces (door, handle, buttons) with 70% ethanol
6. Wash the cell culture dishes and 6-well dishes twice with distilled water Place the in the clean and separated bags to avoid contamination
7. Place the samples after tests in the seal and autoclave-able bags
8. Autoclave all material that is previously specified to be put in autoclave-able bags

Storage

The specimens will be stored in a freezer at $-28°C$ after their arrival and awaiting their transportation.

Disposal

All specimens and accumulated waste materials will be disposed according to the locally relevant protocols at the *Kavli Nanolabs* and *Biomaterials Lab*

Contact information

- Dominique Fuchs (⬛⬛⬛⬛⬛⬛⬛⬛⬛⬛) (Author of the protocol)
- Marc Zuiddam (⬛⬛⬛⬛⬛⬛⬛) (Kavli Nanolabs)
- Monique Schoeman (⬛⬛⬛⬛⬛⬛) (LUMC)

Appendix B - Photos of test-setup & Laboratory

Image B1– Look at the Atomic Force Microscope scanner head through the protective cover at Kavli Nanolabs.
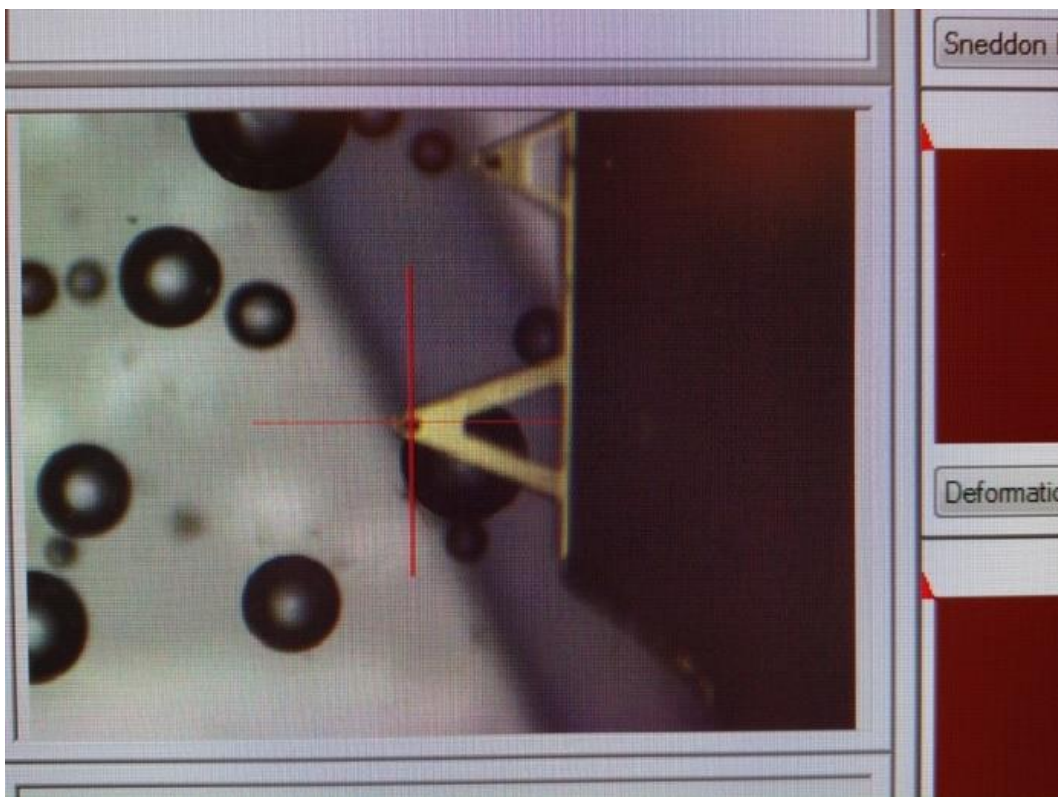
Image B2 – Microscope screen showing the probe head during calibration and artefacts caused by suspended air-bubbles.
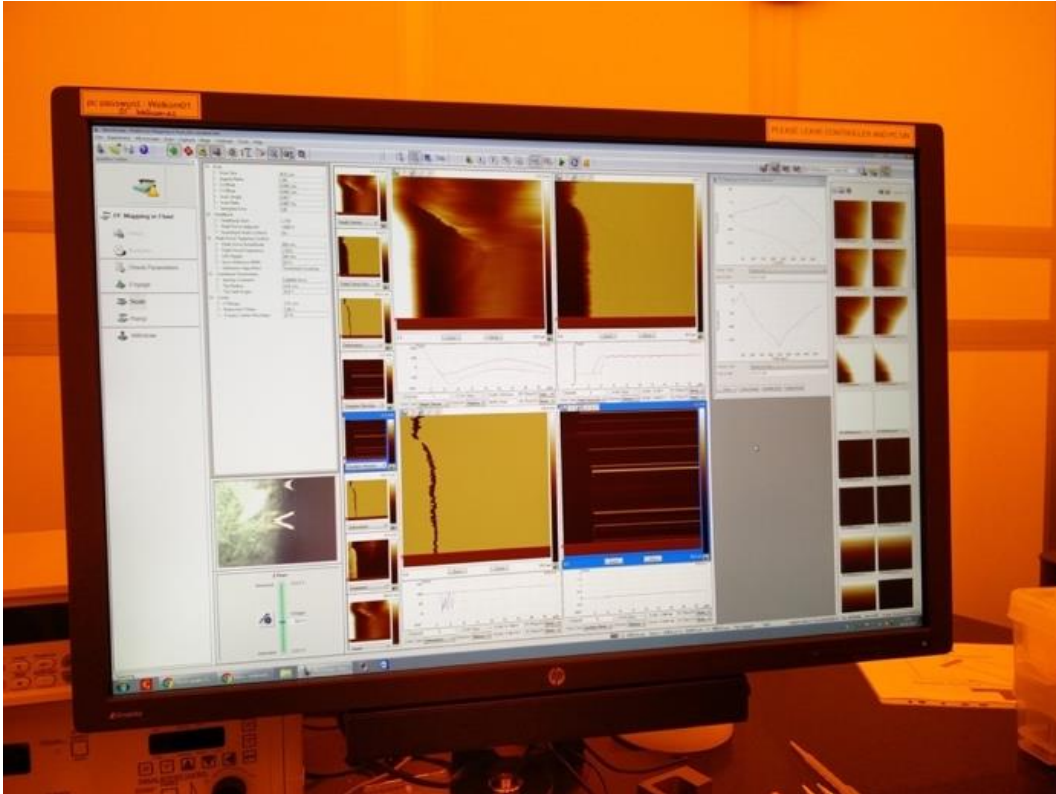
Image B3 – Bruker Nanoscope screen during preliminary experiments. Appendix C - Clustering Indexes

Appendix C - Clustering Indices

Calinski-Harabaz Index

The Calinski-Harabaz index is defined as follows:

$$CH(k) = \frac{Tr(B_K)}{Tr(W_K)} \times \frac{N-k}{k-1}$$

Where B_K is the between group dispersion matrix, and W_K is the within-cluster dispersion matrix defined by:

$$W_K = \sum_{i=1}^{k} \sum_{x \in C_i} (x - c_i)(x - c_i)^T$$

$$B_K = \sum_i n_i (c_i - c)(c_i - c)^T$$

With N being the number of points in the data, C_i the set of points in cluster q, c_i the center of the cluster q, c as the center of E, n_i as the number of points in cluster i.

A higher Calinski-Harabaz score relates to better defined clusters according to the index.

Davies-Bouldin Index

The Davies-Bouldin Index is defined as follows:

$$DB(k) = \frac{1}{k} \sum_{i=1}^{k} D_i$$

Where:

$$D_i = \max_{j=1..k, i \neq j} (R_{ij}), \qquad i = 1..k$$

$$R_{ij} = \frac{s_i + s_j}{d_{ij}}$$

$$d_{ij} = d(v_i, v_j), \quad s_i = \frac{1}{\|c_i\|} \sum_{x \in c_i} d(x, v_i)$$

- $d(x, y)$ is the Euclidian distance between x and y.
- c_i is the cluster i.
- v_i is the centroid of cluster c_i.
- $\|c_i\|$ refers to the norm of c_i.

A lower Davies-Bouldin score equates a better clustering fit according to the index.

Silhouette Coefficient

The silhouette coefficient for a single sample is defined as:

$$s = \frac{b-a}{\max(a,b)}$$

where a is the mean distance between a sample and all other points in the same cluster, and b is the mean distance between a sample and all other points in the next nearest cluster.

The silhouette coefficient of a set of samples is the mean of the silhouette coefficients of all samples.

A higher silhouette score equates a better fitting model according to the silhouette coefficient.

Appendix D - Additional Plots
GMM Fitting of different # of optimal components:
These two examples show that more than 2 components do not necessarily mean that the results more clearly represent the histogram during analysis. For $C_3 t_2$ the increase makes it harder to find the higher stiffness component among the different components, although the fit does increase.
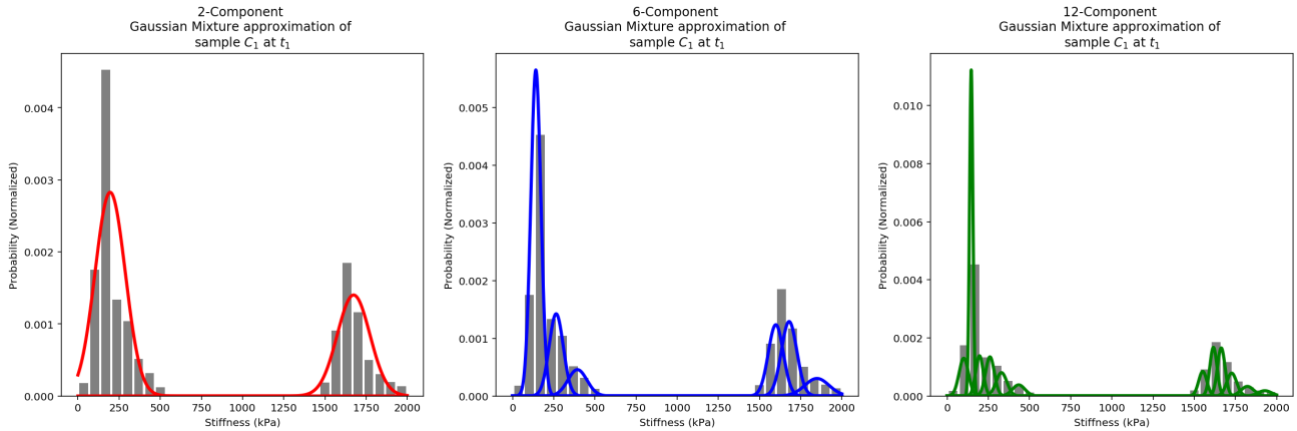
Figure 15 - Gaussian Mixture Model approximations with different number of components (2,6,12) applied to sample $C_1 t_1$.
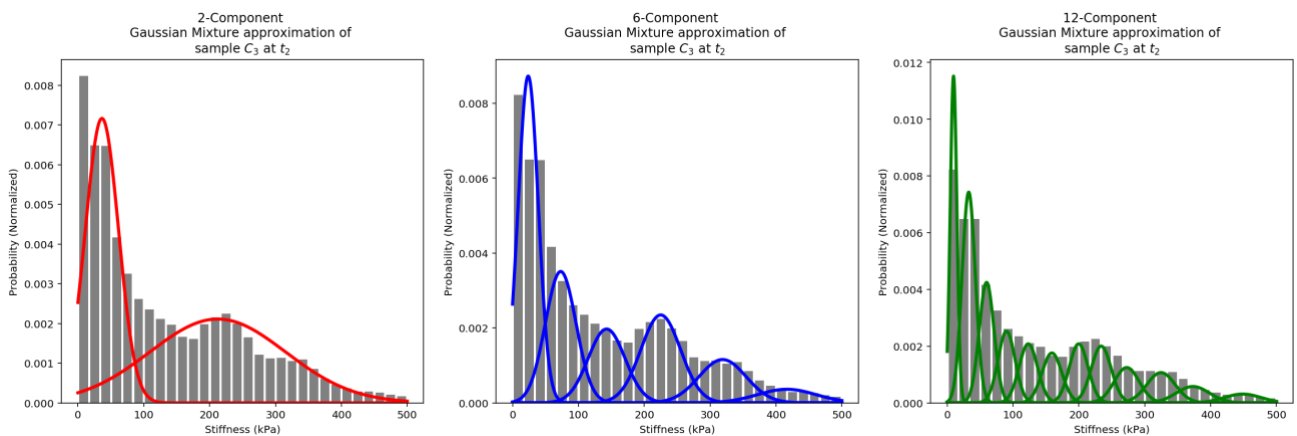
Figure 16 - Gaussian Mixture Model approximations with different number of components (2,6,12) applied to sample $C_3 t_2$.

All Gaussian Components split by sample type and component number.
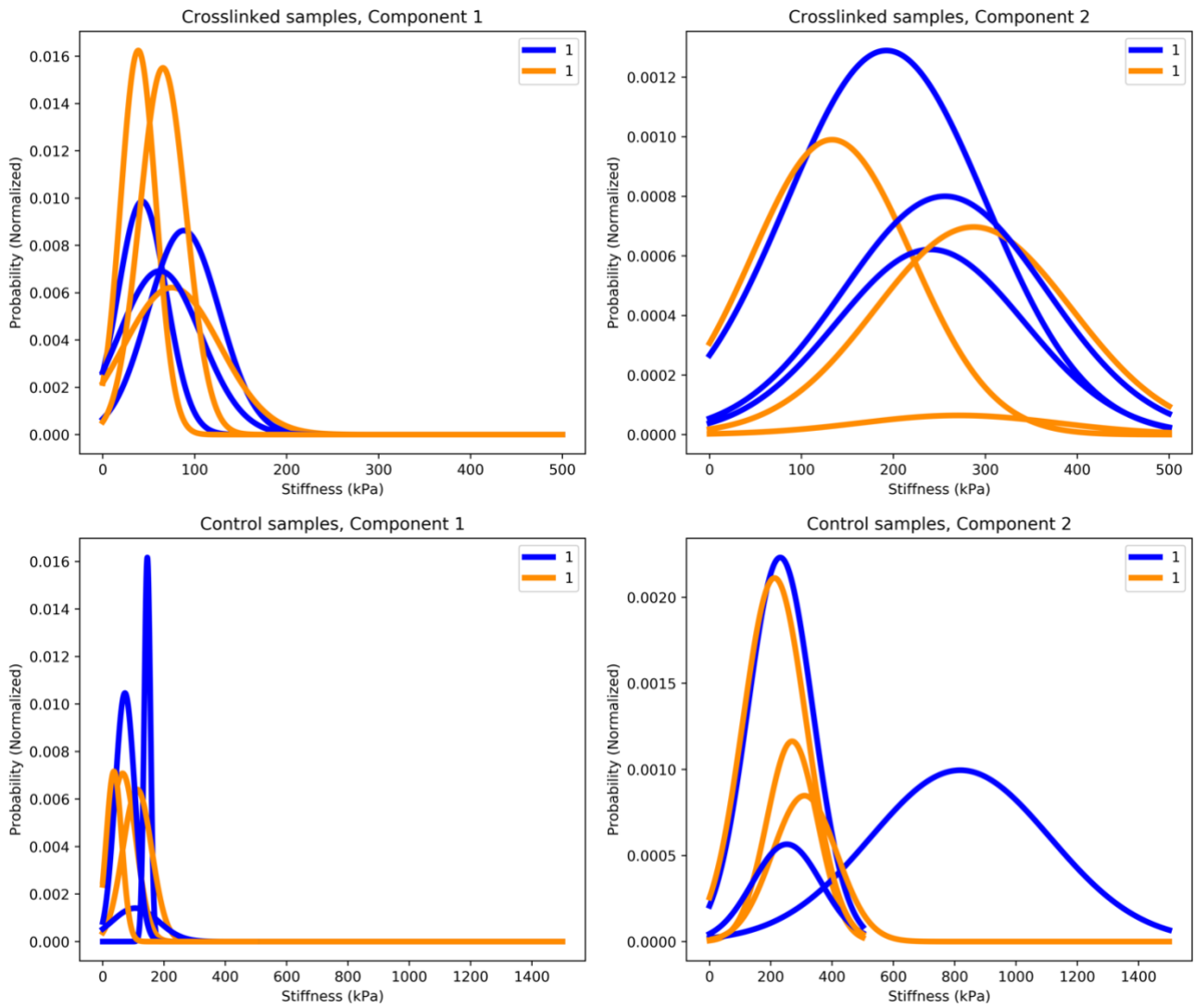
Figure 17 – Separate plots of all Gaussian components, plotted for control and crosslinked samples separately, as well as separately for component 1 and component 2.